



Pyrazolo[1,5a]pyrimidines as a new class of *FUSE* binding protein 1 (FUBP1) inhibitors



Stefanie Hauck^{a,†}, Kerstin Hiesinger^{b,†}, Sabrina Khageh Hosseini^a, Janosch Achenbach^b, Ricardo M. Biondi^{c,d}, Ewgenij Proschak^{b,*}, Martin Zörnig^{a,d,*}, Dalibor Odadzic^{b,d,‡}

^a Georg-Speyer-Haus, Institute for Tumor Biology and Experimental Therapy, Paul-Ehrlich-Straße 42-44, D-60596 Frankfurt/Main, Germany

^b Institute of Pharmaceutical Chemistry, Goethe University Frankfurt, Max-von-Laue-Str. 9, D-60438 Frankfurt/Main, Germany

^c Department of Internal Medicine I, University Hospital Frankfurt, Theodor-Stern-Kai 7, D-60590 Frankfurt/Main, Germany

^d German Cancer Consortium (DKTK), 69120 Heidelberg, Germany

ARTICLE INFO

Article history:

Received 6 June 2016

Revised 13 August 2016

Accepted 8 September 2016

Available online 14 September 2016

Keywords:

FUBP1

Transcriptional regulator

Pyrazolo[1,5a]pyrimidine

ABSTRACT

The transcriptional regulator *FUSE* binding protein 1 (FUBP1) is aberrantly upregulated in various malignancies, fulfilling its oncogenic role by the deregulation of critical genes involved in cell cycle control and apoptosis regulation. Thus, the pharmaceutical inhibition of this protein would represent an encouraging novel targeted chemotherapy.

Here, we demonstrate the identification and initial optimization of a pyrazolo[1,5a]pyrimidine-based FUBP1 inhibitor derived from medium throughput screening, which interferes with the binding of FUBP1 to its single stranded target DNA *FUSE*. We were able to generate a new class of FUBP1 interfering molecules with in vitro and biological activity. In biophysical assays, we could show that our best inhibitor, compound **6**, potently inhibits the binding of FUBP1 to the *FUSE* sequence with an IC₅₀ value of 11.0 μM. Furthermore, hepatocellular carcinoma cells exhibited sensitivity towards the treatment with compound **6**, resulting in reduced cell expansion and induction of cell death. Finally, we provide insights into the corresponding SAR landscape, leading to a prospective enhancement in potency and cellular efficacy.

© 2016 Published by Elsevier Ltd.

1. Introduction

The transcriptional regulator *FUSE* binding protein 1 (FUBP1) contributes to the tumorigenicity of many different malignancies, including liver cancer^{1–4}, colorectal carcinoma^{5–8}, breast cancer^{9,10} and glioma.^{11,12} We and others identified FUBP1 to be aberrantly overexpressed in hepatocellular carcinoma (HCC) tissue compared to healthy human liver.^{1,3} We demonstrated that FUBP1 expression is required for HCC tumor growth due to its anti-apoptotic and pro-proliferative potential. Concordantly, downregulation of FUBP1 by shRNA sensitizes HCC cells for apoptotic stimuli, including mitomycin c (MMC) and doxorubicin (DOX) treatment.¹

FUBP1 is described as a regulator of several target genes including the proto-oncogene *c-MYC*, the cell cycle inhibitor *p21*, the pro-apoptotic Bcl2 family member *BIK* and the cell cycle regulator

cyclin D2 (*CCND2*).^{1,13–15} The protein binds via its four K-homology (KH) domains to the single-stranded Far UpStream Element (*FUSE*), 1500 base pairs (bps) upstream of the *c-MYC* transcription start. Interaction of FUBP1 with the general transcriptional factor TFIIF facilitates promoter escape of the paused polymerase II (POL II) complex, resulting in *c-MYC* peak-expression. In contrast to its activating role in *c-MYC* and *CCND2* transcription, FUBP1 was described as a repressor of *p21* and *BIK* expression.^{16,17}

Both, the aberrant overexpression of FUBP1 in HCC and other tumor entities, and the presence of a druggable DNA-binding furrow predestine this protein a promising candidate for targeted chemotherapy.¹⁸

Until today, one compound class is known to interact with FUBP1 functionality: benzoyl anthranilic acids.¹⁸ Huth et al. showed that this benzoyl anthranilic acid is able to interact with the hydrophobic region of the KH domain of FUBP1, leading to an impaired DNA-binding. Limitations of this class of compounds tested by Huth et al. included poor solubility and high *K_D* and IC₅₀ values (approximately 350 μM for the best tested inhibitor, Fig. 1A).¹⁸

* Corresponding authors. Tel.: +49 69 798 29301 (E.P.), +49 69 63395 115 (M.Z.).

E-mail addresses: Proschak@pharmachem.uni-frankfurt.de (E. Proschak), Zoernig@gsh.uni-frankfurt.de (M. Zörnig).

† Hauck, S. and Hiesinger, K. contributed equally (both first authors).

‡ Odadzic, D. and Zörnig, M. contributed equally (both last authors).

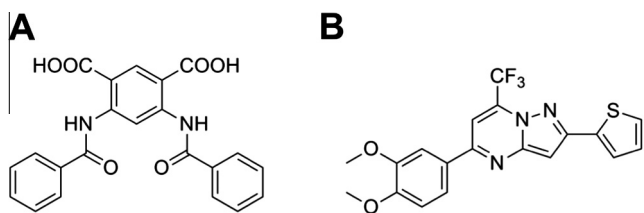


Figure 1. Chemical structures of FUBP1-inhibitors. (A) Best inhibitor from Huth et al. and (B) Compound 6.

Here, we present the results of a structure activity relationship (SAR) study aiming at the identification of a potent FUBP1 inhibitor. The lead structure was identified in a medium throughput screening using AlphaScreen technology. Investigation of pyrazolo[1,5a]pyrimidine derivatives resulted in the identification of compound **6** (Fig. 1B) exhibiting inhibitory activity in *in vitro* and in cellular assays. Thus, we demonstrate the inhibitory potential of pyrazolo[1,5a]pyrimidines on FUBP1 binding to *FUSE* and provide *in silico* analyses of the surface characteristics of the investigated compounds, potentially leading to the generation of an improved FUBP1 inhibitor with increased cellular activity.

2. Results

2.1. Chemistry

The initial SAR landscape was investigated using pyrazolo[1,5a]pyrimidine derivatives commercially available from Maybridge (SAR-by-catalogue). For the second optimization round, a synthetic procedure was established (Figs. 2 and 3).

2.1.1. Synthesis of modified 3(5)-aminopyrazoles

A simple route to obtain pyrazolo[1,5a]pyrimidines is the condensation of a bifunctional nucleophilic, e.g. 1,3-dicarbonyl, with 3(5)-aminopyrazole (Fig. 3).¹⁹ Thus, 3(5)-aminopyrazoles were generated in a three-step protocol. After esterification of the acid moiety with methanol, the resulting methyl ester was substituted by acetonitrile via a Claisen condensation yielding a substituted 3-oxopropanenitrile. The ester substitution represented the limiting step of this synthesis path. For the optimization of this step different parameters of the reaction have been varied. The different procedures are listed in Table 1.^{20–22} In method A, D and E no conversion to the β -ketonitrile could be detected and just educt was re-isolated. The use of acetonitrile and freshly prepared sodium methoxide (method B and C) gave the desired β -ketonitrile with moderate yields. NMR analysis of the isolated product indi-

Table 1
Different approaches for the synthesis of substituted 3-oxopropanenitrile

Method	Solvent	Base	Conditions	Yield
A	Toluene (anhyd)	NaH (3 equiv)	Reflux, 24 h	—
B	ACN (anhyd)	NaOMe (2 equiv)	Reflux, 3 h	24%
C	ACN (anhyd)	NaOMe (2 equiv)	Reflux, 15 h	54%
D	THF (anhyd)	^t BuOK (3 equiv)	rt, 19 h	—
E	THF (technical)	^t BuOK (3 equiv)	rt, 30 min	—

cated traces of the starting material, the acid derivative. Further purification steps were neglected and the substituted 3-oxopropanenitrile was subsequently condensed with hydrazine hydrate in ethanol to generate the 3(5)-aminopyrazole (Fig. 2).

2.1.2. Synthesis of pyrazolo[1,5a]pyrimidine derivatives

After cyclization with hydrazine hydrate, the condensation was performed with a 1,3-dicarbonyl in ethanol. In principle, two possible constitutional isomers are formed depending on the reaction conditions and on the nature of the β -diketone (Fig. 3). In this work, an unsymmetrical 1,3-diketone containing a CF_3 -group was used. This led to the generation of two different enols.²³ For isomer determination, ¹³C NMR spectroscopy was used. According to Emelina²⁴, the C^7CF_3 (Fig. 3A) shows a characteristic signal (quartet) at 133 ppm, whereas C^5CF_3 (Fig. 3; indicated with B) exhibits a signal at approximately 146 ppm. All compounds showed the characteristic C^7CF_3 signal.

2.2. Screening and efficacy evaluation of pyrazolo[1,5a]pyrimidines in *in vitro* and cell culture-based assays

2.2.1. Assay development

To identify a novel FUBP1-inhibitor class, we screened 14,400 small molecules (Maybridge Hit Finder™ library) in an initial Amplified Luminescent Proximity Homogeneous Assay (ALPHA) screen assay for their potential to inhibit the binding between FUBP1 and its target *FUSE* DNA element of the *p21* upstream regulatory region (*FUSE p21*).

In our AlphaScreen experiments, recombinant FUBP1 was coupled to protein-A acceptor beads using the anti-FUBP1 (N15) antibody. The bead-coupled FUBP1 was incubated with DMSO as a control or with compound and a biotinylated *FUSE* oligonucleotide, coupled to streptavidin donor beads (see Section 5 for detailed description). Cross-titrations revealed a concentration-dependent increase in counts for FUBP1 binding to *FUSE p21* (Suppl. Fig. 1A and B). In a proof-of-principle experiment, a dilution series of free *FUSE p21* oligonucleotide was used to compete with the binding of FUBP1 to biotinylated, bead-bound *FUSE p21* (Suppl. Fig. 1C). With

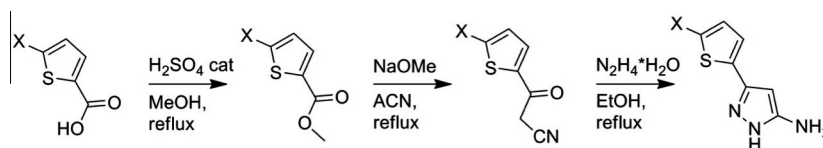


Figure 2. Synthesis of modified 3(5)-aminopyrazole.

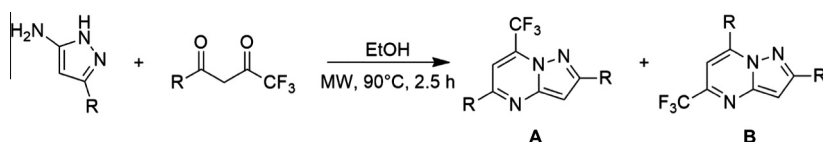


Figure 3. Synthesis of pyrazolo[1,5a]pyrimidine derivatives.

this experiment, we could demonstrate the feasibility of the AlphaScreen assay for the screening of compounds that interfere with the binding of FUBP1 to *FUSE p21* DNA.

All 103 positive hits, exhibiting 30% or less FUBP1/*FUSE p21* binding compared to DMSO control, were rescreened. The most promising candidates were verified using surface plasmon resonance (SPR) technology. In SPR experiments, single stranded biotinylated *FUSE p21* oligonucleotide was immobilized on the gold surface of NLC chips. Upon binding of FUBP1 (liquid phase) to the immobilized *FUSE p21*, response units (RUs) increased and the binding was detected in the association phase. We successfully verified the specific binding of recombinant FUBP1 to the *FUSE p21* oligonucleotide (54 bps), whereas a non-FUBP1 binding single-stranded DNA sequence exhibited no specific increase in RUs (Suppl. Fig. 2). Vice versa, a non-DNA binding protein (Green Fluorescent Protein; GFP) showed no interaction with either *FUSE p21* or the DNA control channel (non-FUBP1 binding single stranded DNA control; see Section 5).

In contrast to AlphaScreen assays, SPR relies on the size change of the SPR chip surface which occurs upon binding of FUBP1 to the immobilized *FUSE p21* oligonucleotide, and not a change in color emission. Therefore, SPR represents a valid complementary assay for the AlphaScreen technology used.

Among the verified small molecule inhibitors, we were able to identify a pyrazolo[1,5*a*]pyrimidine as a reasonable FUBP1 inhibitor (compound **1**; Table 2).

To evaluate the SAR landscape of compound **1**, 16 derivatives were purchased and tested for their inhibitory potential on the FUBP1/*FUSE p21* interaction in an AlphaScreen assay (compounds **2–17**; Table 2). Positive hits were verified using SPR. The compounds exhibiting the lowest IC₅₀ values were evaluated with respect to their FUBP1 inhibition in cell culture-based assays. For this purpose, the change in FUBP1 target gene expression was monitored as an indirect readout for the cellular inhibition of the transcriptional regulation induced by FUBP1.

In a first screening approach, compound **1** and its derivatives **2–17** (Table 2) were incubated with both binding partners (FUBP1 and biotinylated *FUSE p21* oligonucleotide) in a final concentration of 100 μM. In the bead-based proximity assay, the lead compound **1** exhibited a reduction of FUBP1 binding to *FUSE p21* down to 22.7% with respect to the DMSO control (Fig. 4A). A similar inhibitory potential was observed for the derivatives **5** (27.8%), **6** (28.4%) and **7** (9.8%). These hits were successfully verified in SPR experiments, in which biotinylated *FUSE p21* was immobilized on the NLC chip with final response units (RUs) of 50. 25 nM FUBP1 was used in the liquid phase as the binding partner. For the verification of inhibitory compounds, FUBP1 was preincubated with either DMSO control or 100 μM positive hit compound (Fig. 4B). All tested compounds showed a reduction in both the association (0–120 s) and the dissociation phases (120–500 s) of FUBP1 binding to *FUSE p21* compared to solvent control, indicating that the binding of FUBP1 to single-stranded *FUSE p21* DNA is impaired.

2.2.2. In vitro and cell culture testing of initial compound 1 derivatives

To assess the respective IC₅₀ values, a dilution series of compounds **1**, **5**, **6** and **7** (0.02–200 μM) were tested in AlphaScreen and SPR assays. Though the inhibitory potential at 100 μM of the initial positive hits from the first derivatisation of compound **1** did not differ, the IC₅₀ value of compound **6** (24 μM in AlphaScreen and 11 μM in SPR experiments; Fig. 5A and B) was significantly lower compared to that of compound **1** (85 μM). The exchange of a thiophene residue in the position R₂ by 4-toluyl (5) or cyclopropyl (7) resulted in a reduction of the inhibitory potential (IC₅₀ values of 85 μM for compound **5** and 103 μM for compound **7**, respectively; see Table 2).

In addition to the decreased binding capacity of FUBP1 to the *FUSE DNA* of *p21* upon incubation with compound **6**, we observed similar effects with another potential *FUSE* sequence, the *FUSE BIK*. Upon investigation of the upstream region of the *BIK* transcription start site, we detected a potential *FUSE* element with a high similarity to the verified *FUSE p21* DNA sequence (Suppl. Fig. 3A). In proof-of-principle experiments a specific binding of FUBP1 to this *FUSE BIK* oligonucleotide could be verified (Suppl. Fig. 3B and C). Most importantly, compound **6** was able to diminish the binding of FUBP1 to the *FUSE* of *BIK* (Fig. 5C).

To test the cellular inhibition of FUBP1 by this new class of inhibitors in human cells, HCC cell lines were treated with the respective compounds and investigated for changes in FUBP1 target gene expression. We previously showed, that a shRNA-mediated knockdown of *FUBP1* leads to increased *p21* and *BIK* expression levels and a decrease in *CCND2* mRNA in Hep3B cells, with the effects on *p21* expression being most prominent.¹ We expected to observe similar effects after incubation of cells with potential FUBP1 inhibitors.

Treatment of the Hep3B cells with compound **5** or **7** did not result in significant changes of the investigated mRNA expression levels (Suppl. Fig. 4). However, in accordance to the efficacy defined in in vitro assays, compound **6** showed a concentration-dependent upregulation of the FUBP1 target genes *p21* and *BIK* in Hep3B cells with significant fold changes of 6.2 and 1.5, respectively, and a significant decrease in *CCND2* (fold change of –2.7), using a compound concentration of 50 μM (Fig. 5D). This tendency could be verified in the hepatocellular carcinoma cell lines Huh7 and HepG2 (Suppl. Fig. 5).

2.2.3. HCC cells are sensitive for compound 6-treatment

As expected from the deregulation of specific FUBP1 target genes, studies in FUBP1-deficient Hep3B cells exhibited a reduced cell proliferation and an increased sensitivity towards apoptotic stimuli.^{1,3} To test if our potential FUBP1 inhibitor causes similar effects, the HCC cell lines Hep3B, HepG2 and Huh7 were treated with compound **6** and investigated for cell expansion, cell cycle distribution and cell death rates.

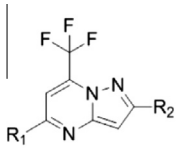
In cell expansion assays, HCC cells were, as mentioned above, either treated with DMSO (solvent control), 10 or 20 μM compound **6** or remained untreated. Cell numbers were quantified after 24, 48 and 72 h (see Section 5). A significantly reduced cell expansion compared to the DMSO-treated control cells was observed 48 and 72 h after treatment of Hep3B with both, 10 and 20 μM of compound **6** (Fig. 6A and B). This effect of compound **6** treatment on the cell expansion of HCC cells could be substantiated by treatment of HepG2 and Huh7 cells. They exhibited an even higher sensitivity towards CPD **6**, with significantly reduced cell proliferation for 10 and 20 μM treatments after 24 h (Suppl. Fig. 6A and B).

The investigation of cell death in Hep3B after 24 h of single-treatment with compound **6** revealed a slight increase in the number of dead cells with both 10 and 20 μM (Fig. 6C and D). This is in line with our previously performed *FUBP1*-knockdown studies, demonstrating that FUBP1-deficiency alone resulted only in minor induction of apoptosis but sensitizes cells for apoptotic stimuli.¹

The combination of our proposed FUBP1 inhibitor compound **6** with MMC or DOX resulted in profound cell killing of Hep3B cells (Fig. 6D). The combination index (CI) is a commonly used mathematical means for the evaluation of drug effect combinations, with values under 1 representing synergism (see Section 5 for detailed description).

Similar tendencies were observed for Huh7 cells and CPD **6** (Suppl. Fig. 6C). The percentage of dead cells was even higher when investigating compound **6**/MMC or compound **6**/DOX treated HepG2 cells, which exhibited no cell death sensitivity towards

Table 2
FUBP1 inhibitory potential of the tested compounds

				Semiquantitative scale: +++++ 0-30 μ M ++++ 30-50 μ M ++ 50-100 μ M + > 100 μ M 0 no detectable activity			
No.	R ₁	R ₂	IC ₅₀ [μ M]	No.	R ₁	R ₂	IC ₅₀ [μ M]
1			++ (85.1)	19			++++ (7.6)
2			0	20			0
3			0	21			0
4			0	22			0
5			++ (84.8)	23			0
6			++++ (11.0)	24			0
7			++ (102.5)	25			+ (ND)
8			0	26			+ (ND)
9			0	27			+ (ND)
10			0	28			+ (ND)
11			0	29			+ (ND)
12			0	30			+ (ND)
13			0	31			++ (ND)
14			0	32			0
15			0	33			0
16			0	34			0
17			0	35			0
18			++++ (11.4)				

(A) All candidate substances were tested in 100 μ M concentrations for their inhibitory potential on the interaction between FUBP1 and the single stranded *FUSE* oligonucleotide of *p21*. ND = not determined.

compound **6** single treatment (Suppl. Fig. 6D). A statistically significant synergism could be observed for all tested combination regimens in HepG2 cells as calculated by the combination index (CI) according to Slinker et al.²⁵

2.2.4. Optimization steps of the hit compound **6**

In order to further increase the inhibitory activity of compound **6** for FUBP1, we investigated derivatives of this molecule with either substitutions in R₁ (keeping the thiophene residue at

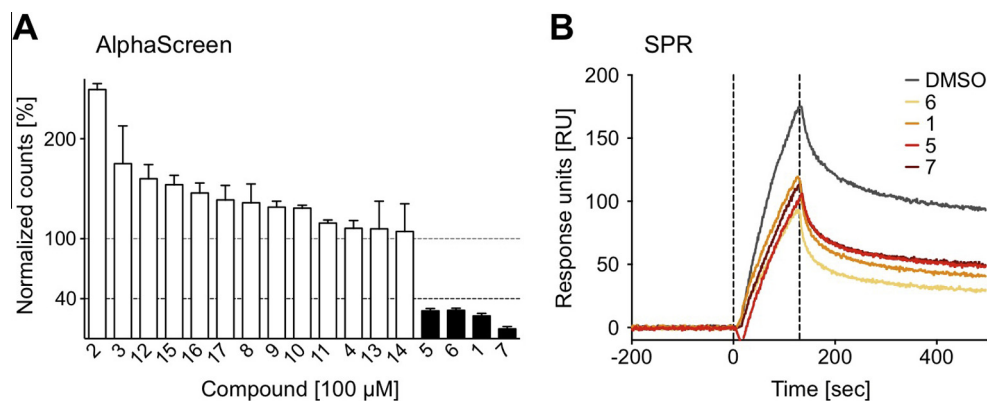


Figure 4. In vitro activity assessment of lead structure (compound 1) derivatives. (A) Compound 1 derivatives were analyzed for their potential to inhibit or prevent the binding between FUBP1 and the *FUSE* DNA of *p21* in an AlphaScreen assay. Compounds with an inhibitory potential of >60% compared to solvent control were defined as positive hits (black bars). (B) Positive AlphaScreen hits were verified using SPR technology. Single-stranded *FUSE p21* DNA (50 RU) was immobilized on a NLC chip surface. 25 nM FUBP1 was incubated with either solvent control (DMSO) or compounds 1, 5, 6 or 7, and response units were normalized to the DNA control channel. Results from one representative experiment out of three independent replicates are shown.

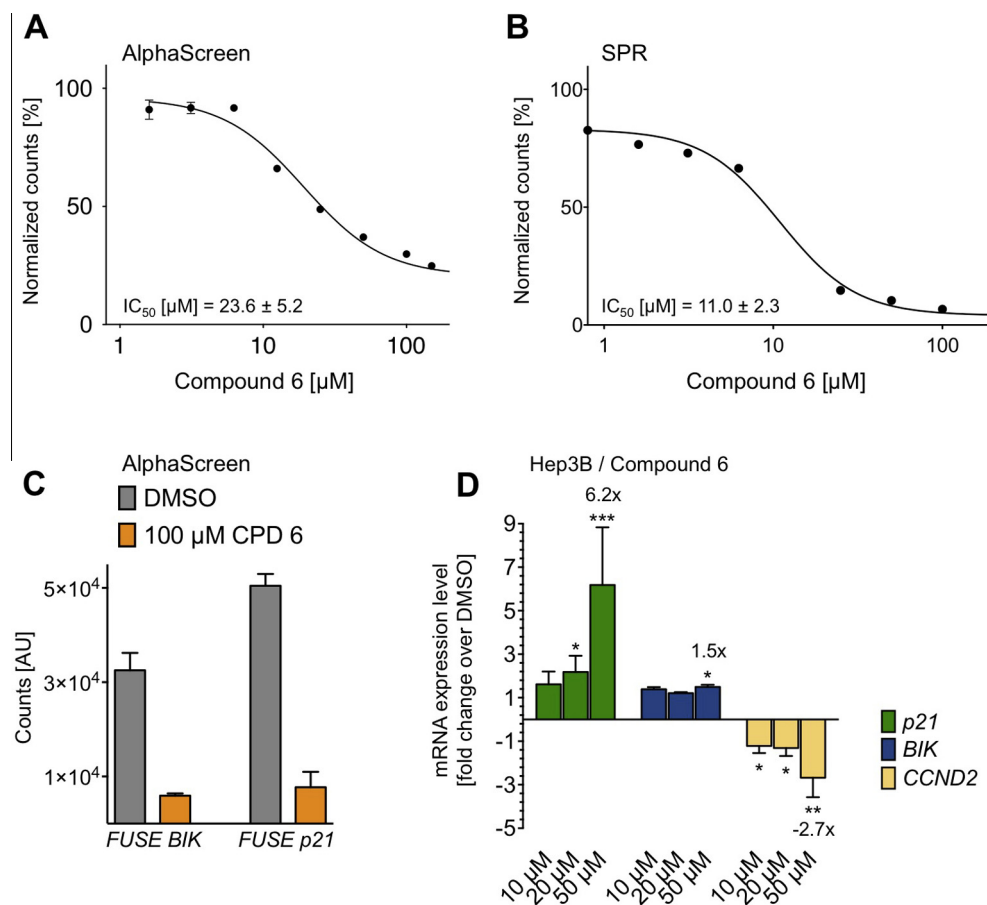


Figure 5. FUBP1/*FUSE* inhibitory efficacy of compound 6. (A and B) IC_{50} determination of compound 6 in AlphaScreen and SPR assays. Compound dilution series (0.1–200 μ M) were performed with 50 nM FUBP1. Binding capacity of FUBP1 to *FUSE p21* was assayed. Data were normalized to the DMSO control. IC_{50} values were calculated from three independent experiments, data show representative curves. (C) Compound 6 potentially prevents the binding of FUBP1 to the *FUSE* of *p21* and the *FUSE* of *BIK*. 100 μ M of compound 6 was preincubated with FUBP1 (25 nM) and binding to the *FUSE* of *p21* or *BIK* was measured in the general AlphaScreen set up. Experiments were performed in three independent replicates. (D) As an indirect readout for the cellular inhibition of FUBP1, qRT-PCR of compound 6 treated cells was performed. Hep3B cells were incubated with the indicated concentrations of compound 6 for 6 h prior to RNA preparation and qRT-PCR analysis. FUBP1-target gene expression levels (*p21*, *BIK* and *CCND2*) were normalized to *GAPDH*. Data are presented as mean \pm SD, three independent experiments were performed.

position R_2 , compounds 20–31; Table 2), or we introduced additional halide groups in the thiophene moiety (compounds 18 and 19; Table 2). Furthermore, we evaluated the importance of the thiophene residue in R_1 substituents by reducing the volume of R_2 (compounds 33–35).

All compounds of the second optimization round (compounds 18–35) were examined in a final concentration of 200 μ M in the general SPR screening set up (Fig. 7A). Positive hits were rescreened in an independent experiment with a final compound concentration of 100 μ M (Fig. 7B). Though the first screening

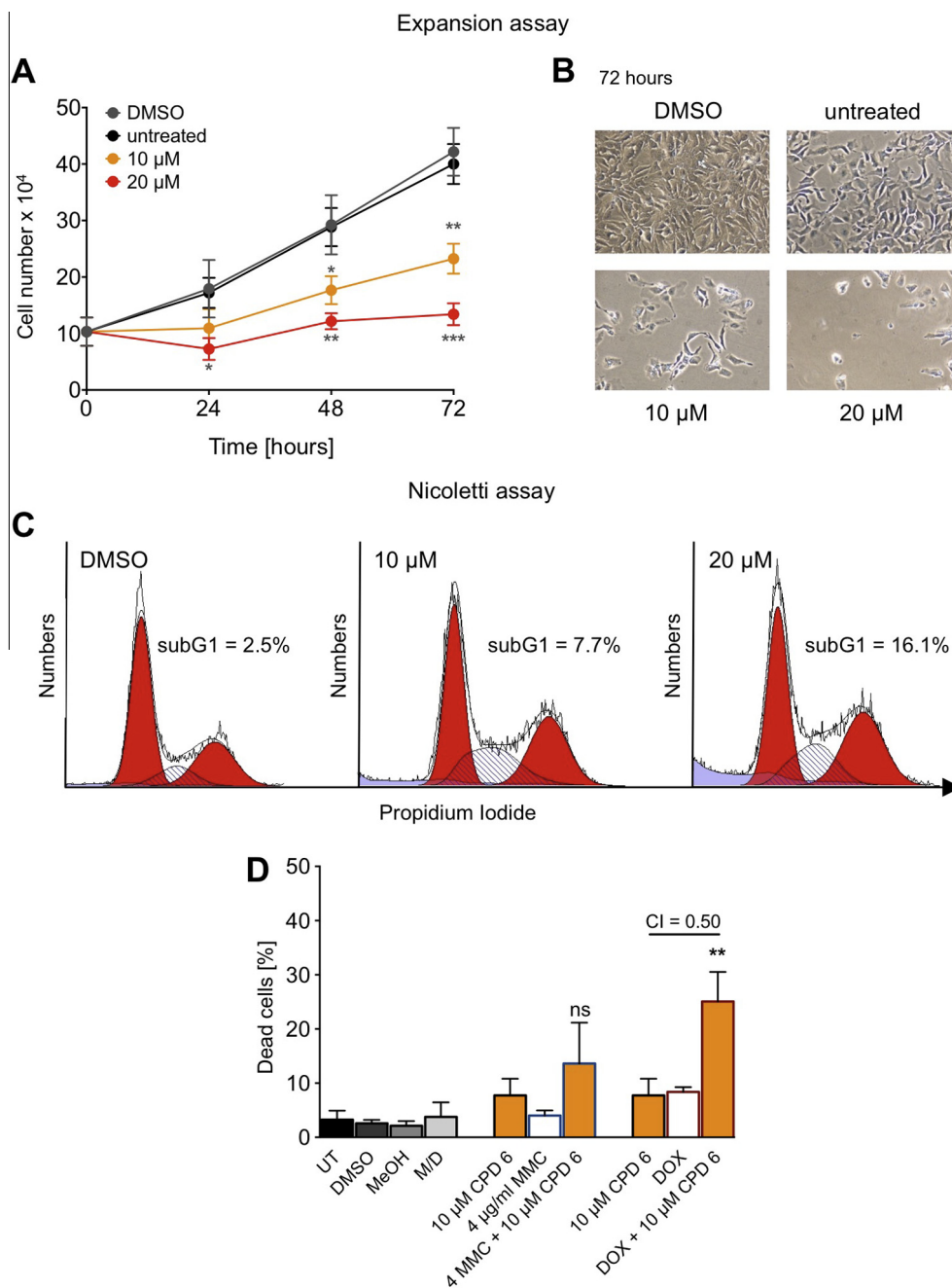


Figure 6. Effects of compound **6** treatment on the proliferation and cell death induction in Hep3B cells. (A) Expansion assays of Hep3B cells, treated with 10 and 20 μM compound **6**, respectively, showed a significantly reduced cell expansion after 48 and 72 h. (B) Light microscopical pictures of untreated, DMSO and compound **6** (10 and 20 μM) treated Hep3B cells after 72 h. (C and D) Nicoletti assay of Hep3B cells, harvested and fixed after 24 h of treatment. 10 and 20 μM of compound **6** treatment resulted in an increase in subG1 cells (dead cells). Representative ModFit analyses of five independent experiments are presented. (D) Upon combination of compound **6** with DOX significant, synergistic cell killing was determined according to combination index analyses. A CI < 1 indicates synergism of the used combinational treatment. Expansion assays were performed in biological triplicates and Nicoletti assays in five biological replicates, each conducted in technical duplicates. UT = untreated; M/D = MeOH/DMSO; MMC = mitomycin c; DOX = doxorubicin; CI = combination index.

resulted in a positive inhibitory potential for 9 out of the 18 tested compounds, the rescreening revealed a potent reduction of FUBP1 binding to *FUSE p21* only for compounds **18** and **19**. In small-scale dilution series (200, 100 and 50 μM), an estimated IC₅₀ value of over 100 μM was determined for compounds **25**, **26** and **28–31** (data not shown). All other compounds lacked efficient inhibition of FUBP1 binding to the *FUSE p21* oligonucleotide in the used assay (white bars, Fig. 7A).

Further investigation of compounds **18** and **19** revealed IC₅₀ values that were comparable to that of compound **6** with 11 μM and

8 μM, respectively (Fig. 8A and B). However, after biological evaluation of these two compounds in cell culture experiments, only an upregulation of *p21* could be detected. Effects on *BIK* expression levels were only minor (Fig. 8C and D).

3. Discussion

Upon derivatisation of compound **1**, we were able to improve the in vitro activity of the investigated pyrazolo[1,5a]pyrimidine

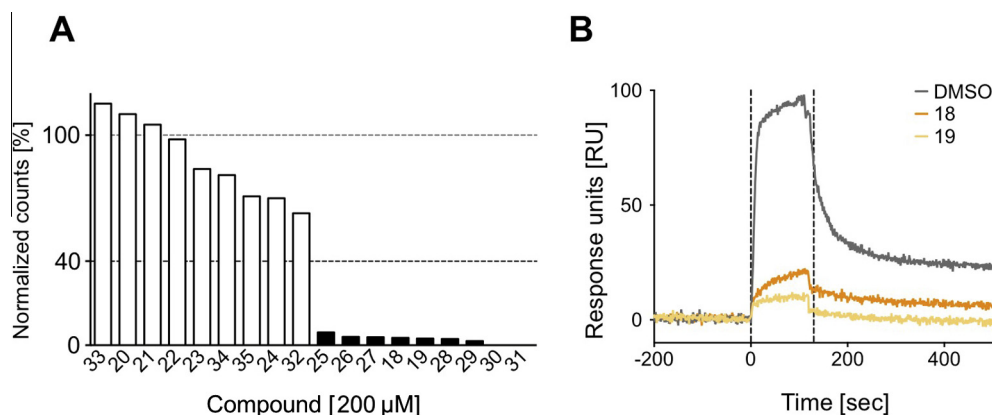


Figure 7. SPR analysis of the potential of compound **6** derivatives to inhibit the FUBP1/*FUSE p21* interaction. (A) Compounds **18–35** were tested at a final concentration of 200 μM with 25 nM FUBP1 protein. Compounds were defined as positive hits with <40% residual FUBP1-binding to *FUSE p21* compared to the DMSO control. (B) Representative binding curves of FUBP1 to *FUSE p21* in the presence of DMSO (solvent control) or compounds **18** and **19**. One representative experiment out of three independent experiments is shown.

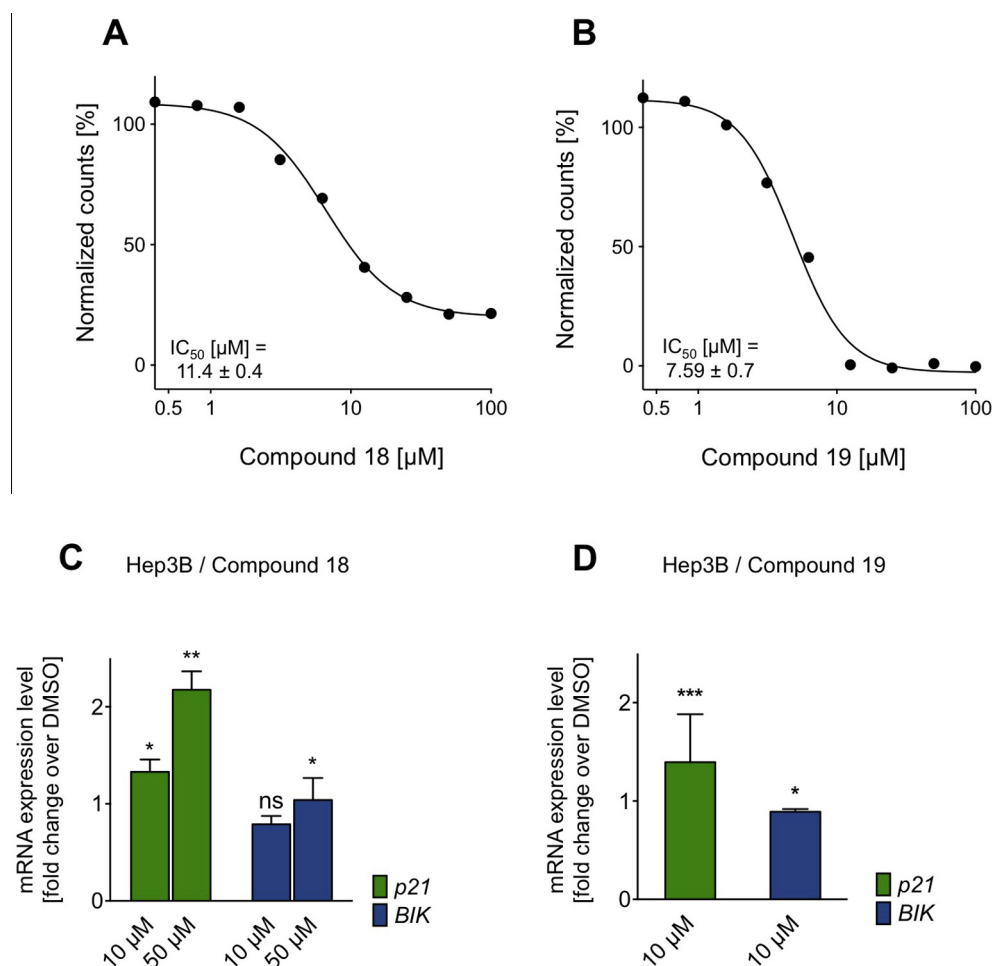


Figure 8. In vitro IC_{50} determination of compounds **18/19** and their influence on FUBP1 target gene expression in HCC cells. Low micromolar IC_{50} values and the deregulation of FUBP1 target genes, as an indirect readout for the cellular inhibition of FUBP1, validate the in vitro inhibitory potential of compounds **18** and **19**. (A and B) The inhibitory concentrations of 50% were calculated from three independent experiments. Results from one experiment are displayed. (C and D) Hep3B cells were incubated with compounds **18** and **19** for 6 h prior to qRT-PCR analysis. Minor but significant fold changes in *p21* were detected. FUBP1-target gene expression levels were normalized to *GAPDH*. Data are presented as mean \pm SD of three independent experiments.

as a FUBP1-inhibitor by 7-fold. Thus, the thiophene moiety and the concomitant increase in hydrophobic surface led to an increase in inhibitory activity (Fig. 9A).

qPCR-analysis revealed a significant upregulation of the direct FUBP1-target gene *p21* in compound **6**-treated HCC cells (Fig. 5D and Suppl. Fig. 5). Additionally, *BIK* and *CCND2* expression levels

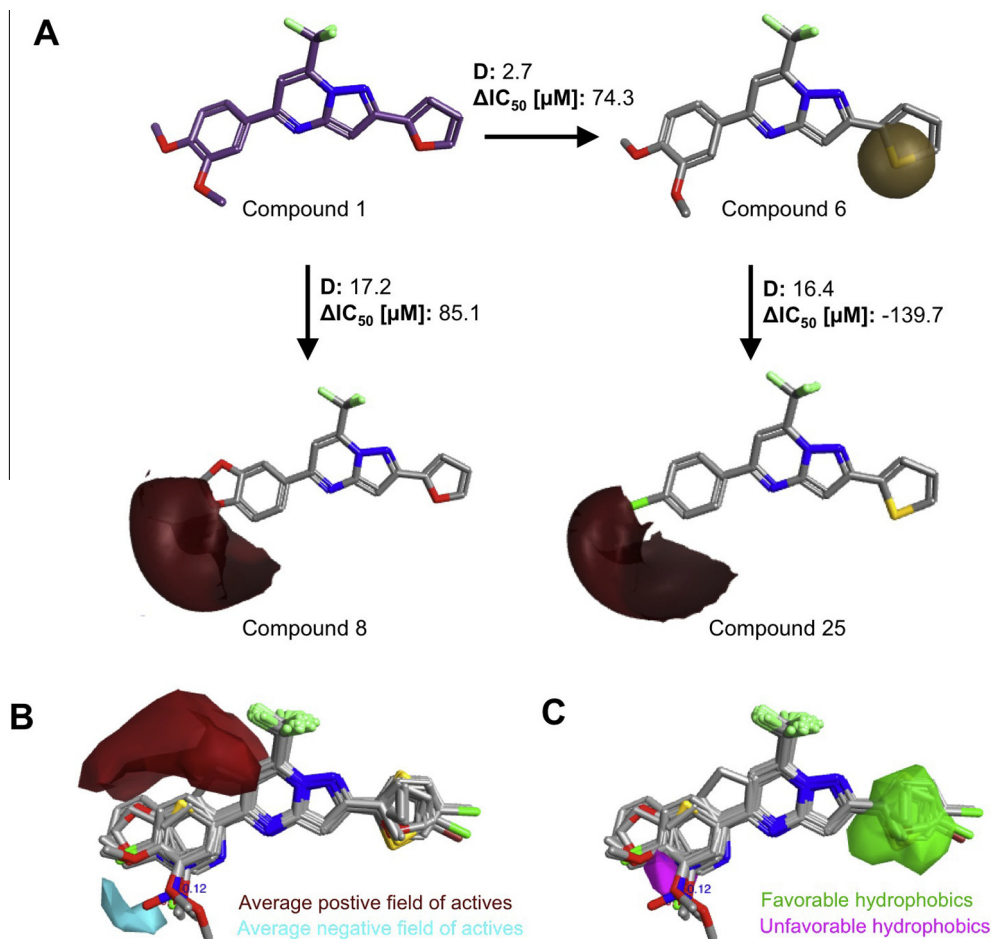


Figure 9. Qualitative analysis of the SAR study using the Activity Minor and Activity Atlas tools from FORGE. (A) 2D structures of all tested SAR molecules were analyzed for their surface polarity and activity, resulting in a disparity calculation for defined pairs of molecules. Differences in the hydrophobic surface and the positive field are depicted in yellow. (B) By comparing active and non-active compounds, favorable and unfavorable hydrophobic regions of this SAR study were assigned using 2D alignment. (C) High disparity regions, represented by the comparison of compound 1/8 and compound 6/25, indicate structurally important areas of the SAR landscape.

changed upon treatment with compound **6** as expected for a FUBP1-inhibiting substance. It is important to note that these kinds of analyses are only an indirect measure of cellular FUBP1 inhibition, which cannot completely exclude the possibility of off-target effects. However, the cellular expansion experiments and the observed sensitization towards apoptotic stimuli correlate well with a cellular FUBP1 inhibition by compound **6** (Fig. 6; Suppl. Fig. 6). Both, FUBP1-deficiency induced by shRNA and treatment with our new class of chemical FUBP1 inhibitor, lead to a decrease in cell expansion, a slight induction of cell death when applied as a monotherapy, and synergistic cell killing in combination with mitomycin c and/or doxorubicin.

The addition of halide groups (compound **18**, **19**) resulted in neglectable changes with respect to the in vitro activity (Fig. 8A and B). However, the biological efficacy was reduced compared to **6** (Fig. 5D; Fig. 8B and C). Changes in the thiophene residue at R₂ correspond to a low disparity value, underlining the flat SAR landscape of this region. Disparity is a common characterization of SAR landscapes, and it includes the structural similarities and functionality of the investigated compounds. High disparities represent pairs of molecules with high similarity and a high difference in efficacy, low disparity values reflect major structural differences without an effect on activity.

While exchanges in R₂, (e.g. addition of heterocyclic groups) were well tolerated, an exchange of R₁ in the lead compound **1**

(which was accompanied by an increase in positive fields) resulted in a complete loss of functionality (Fig. 9A). Even the omission of one of the two methoxy residues led to a significant decrease in activity (compound **1** versus **29/31**; Table 2), as indicated by the high disparity values. The negative electric dipole moment induced by the two methoxy groups seems to be essential for the inhibition of FUBP1 binding to FUSE p21 by pyrazolo[1,5a]pyrimidines (Fig. 9B).

4. Conclusion

Upon optimization of the initial screening hit compound **1** we were able to generate a FUBP1 inhibitor (compound **6**) with a 7-fold decreased IC₅₀ value as determined using in vitro SPR and AlphaScreen assays. The biological activity was demonstrated by FUBP1 target gene deregulation, decreased cell proliferation and increased apoptosis sensitivity.

We could demonstrate that exchanges at position 5 of the pyrazolo[1,5a]pyrimidine scaffold against hydrophobic residues or halogenated aryl groups (e.g. compounds **13**, **17**, respectively **21**, **23**) are unfavorable. Changes at the position 2 of the pyrazolo[1,5a]pyrimidine core, (halide addition of the thiophene residue) highlight the important areas of the SAR landscape. In summary, this preliminary SAR study provides a promising starting point for the generation of a novel, specific and efficient FUBP1-inhibitor.

5. Experimental section

5.1. Materials

The compounds **1–17**, **20**, **22**, **24**, **25**, **27**, **29** and **32–35** were purchased from *Maybridge Chemical Co., Ltd* (Belgium). Chemicals for the synthesis of **18**, **19**, **21**, **23**, **26**, **28**, **30** and **31** were purchased from *Sigma-Aldrich Chemie GmbH* (Steinheim, Germany), *Alfa Aesar GmbH & Co KG* (Karlsruhe, Germany), *Acros Organics* (Geel, Belgium) and *TCl Europe* (Zwijndrecht, Belgium).

The single stranded, biotinylated *FUSE* DNA elements of *p21* and *BIK* used for binding assays (AlphaScreen and SPR) were purchased from *Biospring GmbH* (Frankfurt/Main, Germany).

In this study, the HCC cell lines Hep3B (ATCC no. HB-8064™), HepG2 (ATCC no. HG-8065™) and Huh7 (ATCC no. PTA-4583™) were used.

5.2. Chemistry

5.2.1. General

Reactions were monitored via thin layer chromatography (TLC) using ALUGRAM® from *Merck* (Darmstadt, Germany).

To record NMR-spectra, compounds were dissolved in DMSO-*d*₆ or CDCl₃ and measured on DPX250, Avance 400 and Avance 500 from *Bruker Corporation* (Massachusetts, USA) using tetramethylsilane as an internal standard. All chemical shifts values are reported in ppm, the multiplicity of the signals assigned as follows: s (singlet), d (duplet), t (triplet) and m (multiplet).

Mass spectrometry analysis was performed in positive ion mode by electrospray-ionization (ESI) on a LCMS-2020 single quadrupole MS from *Shimadzu* (Duisburg, Deutschland). Precision mass was measured using MALDI Orbitrap XL from *Life Technologies GmbH* (Darmstadt, Germany).

For purity estimation of the synthesized compounds, a reverse phase high-performance liquid chromatography (RP-HPLC) was performed using the MultoHigh® U-C18 column (50 * 2 mm) from *CS-Chromatographie Service GmbH* (Langerwehe, Germany), and the analysis was conducted using the Shimadzu prominence module from Shimadzu.

Acetonitrile and aqueous formic acid 0.1% was used as eluents. The established method was initiated with 80% water (0.1% formic acid) for 2 min. Then a linear gradient from 80% to 10% water (0.1% formic acid) for 6 min was chosen. After additional 2 min, the gradient again raised to 80% water (0.1% formic acid) within 2 min. The flow rate was adjusted to 0.5 ml/min and the UV-vis detection occurred at 254 nm and 280 nm, respectively.

5.2.2. General procedure for the synthesis of 4,4-trifluoro-1-arylbutane-1,3-dione

Sodium (1.5 equiv) was dissolved under inert conditions in 3–5 ml absolute ethanol, and ethyl trifluoroacetate (2 equiv) (diluted in absolute ethanol) was added. Afterwards, a suitable acetophenone (1 equiv), dissolved in absolute ethanol, was added. The reaction mixture was heated under reflux conditions overnight and cooled to room temperature. Quenching was performed using hydrochloric acid (1 N), and the mixture was stirred for 15 min. After extraction with ethyl acetate, the combined organic phases were washed with brine. The organic layer was dried over MgSO₄, filtrated and the solvent was removed under reduced pressure. The greasy residue was used without any further purification.

5.2.3. Synthesis of methyl-5-halide thiophene-2-carboxylate

5-Halide thiophene-2-carboxylate (1 equiv) was solved in 3 ml absolute methanol, and concentrated sulfuric acid (2.2 equiv) was added. The reaction mixture was heated under reflux conditions

overnight. After cooling to room temperature, the solvent was evaporated. Purified water was added, and the reaction mixture was neutralized with saturated NaHCO₃. After extraction with dichloromethane, the combined organic phase was washed with purified water, 5% NaHCO₃ and brine. The organic layer was dried over MgSO₄ and filtrated. The solvent was removed under reduced pressure, and the white solid phase was used without any further purification.

5.2.3.1. Methyl 5-chlorothiophene-2-carboxylate. For the synthesis of this intermediate, 500 mg (3.08 mmol) 5-chloro thiophene-2-carboxylate, 400 µl (7.5 mmol) sulfuric acid, and 5 ml methanol yielded in 393 mg methyl 5-chlorothiophene-2-carboxylate. Yield: 73%, *R*_f (hexane/ethyl acetate 1:2 v/v): 0.84, ¹H NMR (250 MHz, CDCl₃): δ [ppm] = 7.58 (d, 1H, *J* = 4 Hz, CH_{Ar}), 6.92 (d, 1H, *J* = 4 Hz, CH_{Ar}), 3.87 (s, 3H, CH₃).

5.2.3.2. Methyl 5-bromothiophene-2-carboxylate. For the synthesis of 5-bromothiophene-2-carboxylate 250 mg (1.69 mmol) 5-bromo thiophene-2-carboxylate, 200 µl (3.75 mmol) and 3 ml methanol yielded 310 mg of methyl 5-bromothiophene-2-carboxylate. Yield: 84%, *R*_f (hexane/ethyl acetate 1:1 v/v): 0.9, ¹H NMR (250 MHz, DMSO-*d*₆): δ [ppm] = 7.64 (d, 1H, *J* = 4 Hz, CH_{Ar}), 7.37 (d, 1H, *J* = 4 Hz, CH_{Ar}), 3.82 (s, 3H, CH₃).

5.2.4. Synthesis of 3-(5-halide thiophene-2-yl)-3-oxopropanenitrile

5-halide thiophene-2-carboxylate (1 equiv) was solved under inert conditions in absolute acetonitrile, and sodium methoxide (2 equiv, freshly prepared) was added. The reaction stirred under reflux conditions overnight and was diluted with purified water, afterwards. The aqueous phase was extracted with dichloromethane. The organic layer was dried over MgSO₄, filtrated and the solvent was evaporated under reduced pressure. The white solid phase was used without any further purification.

5.2.4.1. 3-(5-bromothiophene-2-yl)-3-oxopropanenitrile.

The synthesis of this compound was performed with 290 mg (1.33 mmol) methyl 5-bromothiophene-2-carboxylate, 1.5 ml abs. acetonitrile and 1.5 ml (1.78 M) sodium methoxide in methanol and yielded in 166 mg 3-(5-bromothiophene-2-yl)-3-oxopropanenitrile. Yield: 54%, *R*_f (dichloromethane/methanol 9:1 v/v): 0.84, ¹H NMR (250 MHz, DMSO-*d*₆): δ [ppm] = 7.82 (d, 1H, *J* = 4.3 Hz, CH_{Ar}), 7.47 (d, 1H, *J* = 4 Hz, CH_{Ar}), 4.66 (s, 2H, CH₂), ESI-MS (*m/z*): 229.92.

5.2.5. Synthesis of 3-(5-halide thiophene-2-yl)-1H-pyrazol-5-amine/5-(5-halide thiophene-2-yl)-1H-pyrazol-3-amine

Under inert conditions, 3-(5-halogenothiophene-2-yl)-3-oxopropanenitrile (1 equiv) was suspended in ethanol, and hydrazine hydrate (98%; 1.5 equiv) was added. The suspension was heated under reflux overnight, and afterwards, the solvent was evaporated and the residual mixture was solved in dichloromethane. The organic phase was washed with purified water and hydrochloric acid (2.5 M). The acidic phase was neutralized with NaHCO₃ (10% solution) and subsequently extracted with ethyl acetate. This organic phase was dried over MgSO₄, and after filtration, the solvent was removed under reduced pressure.

5.2.5.1. 3-(5-Chlorothiophene-2-yl)-1H-pyrazol-5-amine. For the synthesis of this derivative 300 mg (1.62 mmol) 3-(5-chlorothiophene-2-yl)-3-oxopropanenitrile, 120 µl (2.42 mmol) hydrazine hydrate and 5 ml ethanol yielded in 70 mg of 3-(5-chlorothiophene-2-yl)-1H-pyrazol-5-amine.

Yield: 21%, *R*_f (dichloromethane/methanol 9:1 v/v): 0.59, ¹H NMR (400 MHz, DMSO-*d*₆): δ [ppm] = 11.59 (bs, 1H, NH), 7.08 (d,

1H, $J = 4$ Hz, CHAr), 7.02 (d, 1H, $J = 3.6$ Hz, CHAr), 5.57 (s, 1H, CHAr), 5.04 (s, 2H, NH₂). ESI-MS (m/z): 200.05.

5.2.5.2. 3-(5-Bromothiophene-2-yl)-1H-pyrazol-5-amine. For the synthesis of this compound 150 mg (0.66 mmol) 3-(5-bromothiophene-2-yl)-3-oxopropanenitrile, 49 μ l (0.99 mmol) hydrazine hydrate and 3 ml ethanol yielded in 50 mg of 3-(5-bromothiophene-2-yl)-1H-pyrazol-5-amine.

Yield: 33%, R_f (dichloromethane/methanol 9:1 v/v): 0.60, ¹H NMR (400 MHz, DMSO- d_6): δ [ppm] = 11.73 (bs, 1H, NH), 7.12 (d, 1H, $J = 3.6$ Hz, CHAr), 7.05 (d, 1H, $J = 3.6$ Hz, CHAr), 5.57 (s, 1H, CHAr). ESI-MS (m/z): 243.99.

5.2.6. General procedure for the synthesis of 7-(trifluoromethyl)pyrazolo[1,5-a]pyrimidine

The 1,3-diketone (1 equiv) and the 3-(5)-aminopyrazole (1 equiv) were solved in 3 ml ethanol and heated to 90 °C via microwave irradiation for 2.5 h. After concentration under reduced pressure, the residue was recrystallized in ethanol. A yellow solid was obtained.

5.2.6.1. 2-(5-Chlorothiophene-2-yl)-5-(3,4-dimethoxyphenyl)-7-(trifluoromethyl)pyrazolo[1,5-a]pyrimidine (18).

For the synthesis of this compound 30 mg (0.15 mmol) 3-(5-chlorothiophene-2-yl)-1H-pyrazol-5-amine, 1-(3,4-dimethoxyphenyl)-4,4,4-trifluorobutane-1,3-dione and 3 ml ethanol yielded in 35 mg 3-(5-chlorothiophene-2-yl)-1H-pyrazol-5-amine. Yield: 53%; R_f (hexane/ethyl acetate 2:1 v/v): 0.79; ¹H NMR (400 MHz, CDCl₃): δ [ppm] = 7.79 (d, 1H, $J = 1.2$ Hz, CHAr), 7.62–7.59 (m, 1H, CHAr), 7.53 (s, 1H, CHAr), 7.38 (d, 1H, $J = 3.6$ Hz, CHAr), 6.98 (d, 1H, $J = 8.4$ Hz, CHAr), 6.95 (d, 1H, $J = 4$ Hz, CHAr), 6.91 (s, 1H, CHAr), 4.04 (s, 3H, CH₃), 3.98 (s, 3H, CH₃); ¹³C NMR (100 MHz, CDCl₃): δ [ppm] = 155.3, 152.0, 149.7, 137.0, 130.7, 128.9, 126.4, 125.2, 129.7, 114.3, 111.0, 109.7, 103.3, 93.8, 56.1, 56.1; ESI-MS (m/z): 440.03; HRMS: calculated 440.04419, measured 440.04362 ($\Delta m = 0.00057$, 1.3 ppm).

5.2.6.2. 2-(5-bromothiophene-2-yl)-5-(3,4-dimethoxyphenyl)-7-(trifluoromethyl)pyrazolo[1,5-a]pyrimidine (19).

For the synthesis of this compound 101 mg (0.41 mmol) 3-(5-bromothiophene-2-yl)-1H-pyrazol-5-amine, 1-(3,4-dimethoxyphenyl)-4,4,4-trifluorobutane-1,3-dione and 3 ml ethanol yielded 28 mg 3-(5-bromothiophene-2-yl)-1H-pyrazol-5-amine. Yield: 14%; R_f (hexane/ethyl acetate 5:1 v/v): 0.46; ¹H NMR (400 MHz, CDCl₃): δ [ppm] = 7.99 (d, 1H, $J = 1.2$ Hz, CHAr), 7.62–7.59 (m, 1H, CHAr), 7.54 (s, 1H, CHAr), 7.35 (d, 1H, $J = 4$ Hz, CHAr), 7.09 (d, 1H, $J = 4$ Hz, CHAr), 6.98 (d, 1H, $J = 8.4$ Hz, CHAr), 6.91 (s, 1H, CHAr), 4.04 (s, 3H, CH₃), 3.98 (s, 3H, CH₃); ¹³C NMR (125 MHz, CDCl₃): δ [ppm] = 155.2, 151.9, 150.6, 149.7, 137.0, 133.8 (q, ² $J_{CF} = 37$ Hz, C7), 130.7, 128.9, 126.4, 120.6, 119.5 (q, ¹ $J_{CF} = 272.9$ Hz, CF₃), 114.3, 110.9, 109.6, 103.3 (q, ³ $J_{CF} = 4$ Hz, C6), 93.8, 56.1, 56.1; ¹⁹F NMR (470 MHz, CDCl₃): δ [ppm] = –68.8; purity (HPLC): 96%; ESI-MS (m/z): 486.05; HRMS: calculated 483.99367, measured 483.99338 ($\Delta m = 0.00029$, 0.6 ppm).

5.2.6.3. 5-(3-chlorophenyl)-2-(thiophene-2-yl)-7-(trifluoromethyl)pyrazolo[1,5-a]pyrimidine (21).

For the synthesis of this compound 160 mg (0.97 mmol) 3-(thiophene-2-yl)-1H-pyrazol-5-amine, 1-(3-chlorophenyl)-4,4,4-trifluorobutane-1,3-dione and 2.5 ml ethanol yielded 235 mg 5-(3-chlorophenyl)-2-(thiophene-2-yl)-7-(trifluoromethyl)pyrazolo[1,5-a]pyrimidine.

Yield: 64%; R_f (hexane/ethylacetate 5:1 v/v): 0.73; ¹H NMR (250 MHz, DMSO- d_6): δ [ppm] = 8.38–8.37 (m, 1H, CHAr), 8.31–8.27 (m, 1H, CHAr), 8.21 (s, 1H, CHAr), 7.83–7.82 (m, 1H, CHAr), 7.72–7.58 (m, 3H, CHAr), 7.45 (s, 1H, CHAr), 7.25–7.21 (m, 1H, CHAr);

¹³C NMR (125 MHz, CDCl₃): δ [ppm] = 153.8, 153.2, 150.5, 137.9, 135.4, 135.1, 134.1 (q, ² $J_{CF} = 37.6$ Hz, C7), 131.0, 130.3, 127.9, 127.3, 126.7, 125.2, 120.5, 118.4 (q, ¹ $J_{CF} = 273$ Hz, CF₃), 103.1 (q, ³ $J_{CF} = 4$ Hz, C6), 94.8; ¹⁹F NMR (470 MHz, CDCl₃): δ [ppm] = –68.8; mp = 176.9 °C; purity (HPLC): 99%; ESI-MS (m/z): 379.97; HRMS: calculated 380.02306, measured 380.02286 ($\Delta m = 0.0002$, 0.5 ppm).

5.2.6.4. 5-(4-fluorophenyl)-2-(thiophene-2-yl)-7-(trifluoromethyl)pyrazolo[1,5-a]pyrimidine (23).

100 mg (0.61 mmol) GP5, 3-(thiophene-2-yl)-1H-pyrazol-5-amine, 1-(4-fluorophenyl)-4,4,4-trifluorobutane-1,3-dione and 2.5 ml ethanol yielded in 62 mg 5-(4-fluorophenyl)-2-(thiophene-2-yl)-7-(trifluoromethyl)pyrazolo[1,5-a]pyrimidine. Yield: 38%; R_f (hexane/ethyl acetate 3:1 v/v): 0.87; ¹H NMR (400 MHz, CDCl₃): δ [ppm] = 8.40–8.36 (m, 2H, CHAr), 8.10 (s, 1H, CHAr), 7.81–7.79 (m, 1H, CHAr), 7.70–7.68 (m, 1H, CHAr), 7.43–7.83 (m, 3H, CHAr), 7.23–7.21 (m, 1H, CHAr); ¹³C NMR (125 MHz, CDCl₃): δ [ppm] = 158.3 (q, ² $J_{CF} = 36.5$ Hz), 152.6, 152.3, 150.0, 148.6, 144.8, 134.2, 133.0 (q, ² $J_{CF} = 36.5$ Hz, C7), 128.4, 127.9, 122.1, 119.4 (q, ¹ $J_{CF} = 272.9$ Hz, CF₃), 115.7 (q, ¹ $J_{CF} = 290$ Hz, CF), 105.1 (q, ³ $J_{CF} = 3.6$ Hz, C6), 95.3; ¹⁹F NMR (470 MHz, CDCl₃): δ [ppm] = –74.7, –67.6; mp = 191.3 °C; purity (HPLC): 98%; ESI-MS (m/z): 364.00; HRMS: calculated 364.05261, measured 364.05275 ($\Delta m = 0.00014$, 0.4 ppm).

5.2.6.5. 5-(pyridin-4-yl)-2-(thiophene-2-yl)-7-(trifluoromethyl)pyrazolo[1,5-a]pyrimidine (26).

100 mg (0.61 mmol) 3-(thiophene-2-yl)-1H-pyrazol-5-amine, 4,4,4-trifluoro-1-(pyridin-4-yl)butane-1,3-dione and 2.5 ml ethanol yielded in 63 mg of 5-(pyridin-4-yl)-2-(thiophene-2-yl)-7-(trifluoromethyl)pyrazolo[1,5-a]pyrimidine. Yield: 60%; R_f (hexane/ethyl acetate 1:2 v/v): 0.5; ¹H NMR (400 MHz, DMSO- d_6): δ [ppm] = 8.93 (d, 2H, $J = 5.6$ Hz, CHAr), 8.48 (d, 2H, $J = 4$ Hz, CHAr), 8.34 (s, 1H, CHAr), 7.87 (d, 1H, $J = 2.8$ Hz, CHAr), 7.73 (d, 1H, $J = 4.8$ Hz, CHAr), 7.59 (s, 1H, CHAr), 7.25–7.23 (m, 1H, CHAr); ¹³C NMR (125 MHz, DMSO- d_6): δ [ppm] = 165.7, 163.7, 154.3, 153.0, 150.6, 135.2, 134.1 (q, ² $J_{CF} = 37.1$ Hz, C7), 132.4, 129.3, 127.9, 127.2, 126.6, 119.4 (q, ¹ $J_{CF} = 273$ Hz, CF₃), 116.2, 103.0 (q, ³ $J_{CF} = 4.1$ Hz, C6), 94.6; ¹⁹F NMR (470 MHz, DMSO- d_6): δ [ppm] = –68.8; purity (HPLC): 98%; ESI-MS (m/z): 347.00; HRMS: calculated 347.05728, measured: 347.05746 ($\Delta m = 0.00018$, 0.5 ppm).

5.2.6.6. 5-(pyridin-3-yl)-2-(thiophene-2-yl)-7-(trifluoromethyl)pyrazolo[1,5-a]pyrimidine (28).

100 mg (0.61 mmol) 3-(thiophene-2-yl)-1H-pyrazol-5-amine, 4,4,4-trifluoro-1-(pyridin-3-yl)butane-1,3-dione and 3 ml ethanol yielded 76 mg 5-(pyridin-4-yl)-2-(thiophene-2-yl)-7-(trifluoromethyl)pyrazolo[1,5-a]pyrimidine. Yield: 24%; R_f (hexane/ethyl acetate 1:2 v/v): 0.36; ¹H NMR (400 MHz, DMSO- d_6): δ [ppm] = 9.47 (s, 1H, CHAr), 8.76 (d, 1H, $J = 4.4$ Hz, CHAr), 8.66 (d, 1H, $J = 7.6$ Hz, CHAr), 8.23 (s, 1H, CHAr), 7.83 (d, 1H, $J = 2.8$ Hz, CHAr), 7.71 (d, 1H, $J = 4.8$ Hz, CHAr), 7.64–7.60 (m, 1H, CHAr), 7.47 (s, 1H, CHAr), 7.24–7.22 (m, 1H, CHAr); ¹³C NMR (125 MHz, CDCl₃): δ [ppm] = 153.3, 152.9, 151.8, 150.6, 148.5, 135.0, 134.5, 134.3 (q, ² $J_{CF} = 37.6$ Hz, C7), 131.9, 127.9, 127.4, 126.8, 123.8, 119.4 (q, ¹ $J_{CF} = 273$ Hz, CF₃), 102.9 (q, ³ $J_{CF} = 3.8$ Hz, C6), 95.0; ¹⁹F NMR (470 MHz, CDCl₃): δ [ppm] = –68.8; purity (HPLC): 97%; ESI-MS (m/z): 346.99; HRMS: calculated 347.05728, measured 347.05812 ($\Delta m = 0.00084$, 2.4 ppm).

5.2.6.7. 5-phenyl-2-(thiophene-2-yl)-7-(trifluoromethyl)pyrazolo[1,5-a]pyrimidine (30).

76 mg (0.46 mmol) 3-(thiophene-2-yl)-1H-pyrazol-5-amine, 4,4,4-trifluoro-1-phenylbutane-1,3-dione and 3 ml ethanol yielded 80 mg 5-(pyridin-4-yl)-2-(thiophene-2-yl)-7-(trifluoromethyl)pyrazolo[1,5-a]pyrimidine. Yield: 50%; R_f (hexane/ethylacetate 5:1 v/v): 0.75; ¹H NMR (250 MHz,

DMSO- d_6): δ [ppm] = 8.36–8.29 (m, 2H, CH_{Ar}), 8.12 (s, 1H, CH_{Ar}), 7.83–7.80 (m, 1H, CH_{Ar}), 7.71–7.69 (m, 1H, CH_{Ar}), 7.63–7.58 (m, 3H, CH_{Ar}), 7.42 (s, 1H, CH_{Ar}), 7.24–7.21 (m, 1H, CH_{Ar}); ¹³C NMR (125 MHz, DMSO- d_6): δ [ppm] = 155.3, 152.0, 150.0, 135.5, 134.5, 134.1 (q, ²J_{CF} = 36.5 Hz, C7), 131.2, 129.0, 128.2, 127.9, 127.4, 119.4 (q, ¹J_{CF} = 273 Hz, CF₃), 104.6 (q, ³J_{CF} = 3.8 Hz, C6), 94.3; ¹⁹F NMR (470 MHz, DMSO- d_6): δ [ppm] = –67.5; mp = 161.9 °C; purity (HPLC): 99%; ESI (*m/z*): 346.08; HRMS: calculated 346.06203, measured 346.06225 (Δm = 0.00022, 0.6 ppm).

5.2.6.8. 5-(3-methoxyphenyl)-2-(thiophene-2-yl)-7-(trifluoromethyl) pyrazolo[1,5a]pyrimidine (31). 100 mg (0.61 mmol) 3-(thiophene-2-yl)-1H-pyrazol-5-amine, 4,4,4-trifluoro-1-(3-methoxyphenyl)butane-1,3-dione and 2.5 ml ethanol yielded 52 mg 5-(3-methoxyphenyl)-2-(thiophene-2-yl)-7-(trifluoromethyl)pyrazolo[1,5-a]pyrimidine.

Yield: 23%; *R_f* (hexane/ethyl acetate 3:1 v/v): 0.63; ¹H NMR (400 MHz, CDCl₃): δ [ppm] = 8.12 (s, 1H, CH_{Ar}), 7.89 (d, 1H, *J* = 8 Hz, CH_{Ar}), 7.83–7.80 (m, 2H, CH_{Ar}), 7.71–7.69 (m, 1H, CH_{Ar}), 7.47 (t, 1H, *J* = 8 Hz, CH_{Ar}), 7.42 (s, 1H, CH_{Ar}), 7.24–7.21 (m, 1H, CH_{Ar}), 7.17–7.15 (m, 1H, CH_{Ar}), 3.86 (s, 3H, CH₃); ¹³C NMR (125 MHz, DMSO- d_6): δ [ppm] = 159.7, 155.1, 152.0, 149.9, 136.9, 134.4, 132.6 (q, ²J_{CF} = 37 Hz, C7), 130.1, 128.1, 127.8, 127.4, 119.8, 117.2, 112.2, 104.7 (q, ³J_{CF} = 4.1 Hz, C6), 94.3, 55.3; ¹⁹F NMR (470 MHz, CDCl₃): δ [ppm] = –67.5; ESI-MS (*m/z*): 376.03; HRMS: calculated 376.07259, measured 376.07313 (Δm = 0.00054, 1.4 ppm).

5.3. Evaluation of pyrazolo(1,5a)pyrimidine derivatives in vitro and in cell culture experiments

5.3.1. FUBP1 protein expression from *Escherichia coli* and human HEK293T cells

Human full-length FUBP1 cDNA sequence (codon-optimized for expression in *E. coli*; coFUBP1) was purchased from GenScript (New Jersey, USA). The coFUBP1 sequence was cloned into the bacterial expression vector pET28b with a C-terminal hexahistidine tag (6xHis) under the control of a T7 promoter. Expression of coFUBP1 in the *E. coli* bacteria strain BL21(DE3) was induced via a published auto-induction protocol.²⁶ A freshly prepared overnight culture was diluted 1:100 to inoculate the main culture in a 10 l fermenter. Cells were grown to an optical density (OD₆₀₀) of 0.8. Afterwards, the temperature was reduced from 37 °C to 22 °C, and cells were grown for 35 h before harvesting. To prevent excessive foam formation, 2 ml anti-foam were added daily. The ventilation of the system was ensured by a constant airflow between 4 and 12 l/min.

For cell lysis, the bacterial pellet from a 5 L auto-induced bacterial cell suspension was resuspended in lysis buffer (50 mM MES pH 6.5, 50 mM NaCl), including Complete EDTA free Protease Inhibitor Cocktail (Roche, Mannheim, Germany) and DNase I (Sigma-Aldrich). Subsequently, the cell suspension was processed in the Constant Cell Disruption System (Constant System Limited, Northants, United Kingdom) using a three-step protocol. The cell suspension was applied with a pressure of 1 kbar, followed by two runs at 2 kbar. All steps were performed at 4 °C. The soluble protein fraction was separated from cell debris using a 50 min centrifugation step (20,000×g; 4 °C).

For eukaryotic expression in HEK293T cells, the huFUBP1 coding sequence with an additional 6xHis tag was cloned into the pcDNA3.1(+) vector (Invitrogen, Darmstadt, Germany). Cells were transfected using polyethyleneimine (Sigma-Aldrich), harvested after two days of protein production and lysed using the following lysis-buffer: 50 mM Tris pH 7.4, 0.26 M sucrose, 1 mM Na-orthovanadate, 1 mM EDTA, 1 mM EGTA, 10 mM Na-β-glycerolphosphate, 50 mM NaF, 5 mM Na-pyrophosphate and 1% Triton-X-100.

5.3.2. FUBP1 protein purification by IMAC and Heparin affinity chromatography

The following purification steps were performed at 4 °C, using the Äkta purifier® system (GE Healthcare, Munich, Germany). The cell lysate prepared with the Constant Cell Disruption System (see above) was centrifuged at 20,000×g for 1 h, before it was loaded onto a self-packed Omnifit® Chromatography Column (Diba Industries, Danbury, USA) with Ni-Sepharose High Performance affinity media for high-resolution (GE Healthcare) at a ratio of 25:1 for bacterially expressed FUBP1 and 140:1 for FUBP1 protein expressed in HEK293T cells and a flow rate of 2.5 ml/min. After absorption of the His-tagged protein, the column was equilibrated with 4 column volumes (CVs) of washing buffer (FUBP1 from *E. coli*: 50 mM MES pH 6.5, 50 mM NaCl, 4 mM imidazole; FUBP1 from HEK293T cells: 50 mM Tris pH 7.4, 0.26 M sucrose, 0.05% (v/v) β-mercaptoethanol, PMSF), using a flow rate of 4 ml/min. Elution of the protein was achieved with an imidazole gradient (2 ml/min), and the protein of interest eluted at approximately 50–60% of the final elution buffer (FUBP1 from *E. coli*: 50 mM MES pH 6.5, 50 mM NaCl, 404 mM imidazole; FUBP1 from HEK293T cells: 50 mM Tris pH 7.4, 0.26 M sucrose, 400 mM imidazole, 0.05% (v/v) β-mercaptoethanol, PMSF), corresponding to an imidazole concentration of 220 mM. Fractions displaying an elution peak at A280 absorption were analyzed by SDS-PAGE.

The FUBP1-containing fractions were pooled and applied to HiTrap heparin HP columns (GE Healthcare), 5 × 5 ml for bacterially expressed FUBP1 and 1 × 5 ml for FUBP1 expressed in HEK293T cells, with a flow rate of 2.5 ml/min for purification of DNA-binding proteins. The column was washed with 10 CVs of heparin washing buffer (50 mM MES pH 6.5, 50 mM NaCl, 3 mM DTT), using a flow rate of 2 ml/min. For elution of the FUBP1 protein, a 3-step gradient of heparin elution buffer (50 mM MES pH 6.5, 2 M NaCl, 3 mM DTT) was applied: 1.: 0–17% of final heparin elution buffer for 51 CVs, 2.: 17–21% for 15 CVs; and 3.: 21–28% for 18 CVs. Identity of recombinant FUBP1 protein was verified by Western Blot using the specific FUBP1 antibody (N-15) and mass spectrometry analysis.

5.3.3. AlphaScreen

For bead-based binding assays of recombinant FUBP1 to the FUSE of *p21* (FUSE *p21*; 5'-CTG GCT TTT TGT TTT CAT TTT GTT TTT TTG TTT TGT TTT GTT TTT TGA GAC AA-3') or the FUSE of *BIK* (FUSE *BIK*; 5'-CTT TTG TGG GGT TTT TTT GTT TGT TTT TGT TTT TGT TTT TTT GA-3'), the AlphaScreen™ General IgG (Protein A) Detection Kit from Perkin Elmer was used (Massachusetts, USA). FUSE *p31* was used as a negative control (5'-CAG CCC TGG CTT TTT GTT TTC ATT T-3').

To identify optimal assay conditions for a subsequent analysis of small molecules, cross titrations of purified FUBP1 (*E. coli* expression system) and different FUSE elements were performed. The assay buffer contained 100 mM Tris pH 7.4, 50 mM NaCl, 0.1% BSA, 0.01% Surfact Amp, 4 mM DTT and 1% DMSO. Dilution series of FUBP1 (2.5–40 nM) and FUSE *p21* (0.4–3.2 nM) or FUSE *BIK* (0.4–3.2 nM) were prepared, and 5 μl of each dilution step was transferred to 384-well plates. Beforehand, 5 μl AlphaScreen mix 1 (assay buffer and 3 μM poly dIdC; Sigma-Aldrich Chemie GmbH) were dispensed per well. Prior to a 1 h incubation step at room temperature, 5 μl of the acceptor bead (1:50) and anti-FUBP1 (N-15) antibody (Santa Cruz biotechnology, Heidelberg, Germany) mixture (final concentration of 10 pM) prepared in assay buffer were added. Afterwards, 5 μl of the AlphaScreen donor bead dilution (1:50) in assay buffer was added. The plate was shortly centrifuged, and signals were detected after 20 h at room temperature using the Envision® multiplate reader SN 1040002 (Perkin Elmer). Same conditions were used for the assessment of

FUBP1 (expressed from HEK293T cells) binding to the potential *FUSE* of *BIK* (*FUSE BIK*).

For the medium throughput screening, 50 μM final compound concentration was aliquoted into 384-well plates. A mixture of 3 nM FUBP1 (*E. coli* expression system), 1.6 nM *FUSE p21*, 3 μM poly dIdC, 10 pM anti-FUBP1 (N-15) antibody and acceptor beads (1:50 dilution) were added. After an incubation time of 1 h at room temperature, donor beads (1:50) were added. After an additional incubation period of 20 h, light emission at 520–620 nm was measured using the Envision[®] multilable plate reader from *Perkin Elmer*.

To determine the inhibitory potential of compound **1** derivatives, appropriate FUBP1 (HEK293T expression system) and *FUSE p21* concentrations were chosen, which produced a signal in the exponential phase. If not otherwise stated, the *FUSE* element of *p21* (*FUSE p21*) was used for inhibitor screenings. In a first step, 10 μl of the tested compound dilution (final concentration of 100 μM) was added to the 384-well plate. A master mix containing FUBP1 (26 nM), *FUSE p21* (1.2 nM), poly dIdC (3 μM), anti-FUBP1 N-15 (10 pM), acceptor beads (1:50) and assay buffer was prepared, and 5 μl for each assay point were added. After 1 h at room temperature, 5 μl of a donor bead dilution (1:50) were added and signals were detected after 20 h of incubation. A DMSO control was used as a reference for maximal binding capacity. Positive hits were verified in a second independent experiment, in which a 50 μM concentration point was included.

To assess the IC_{50} value of potential FUBP1 inhibitors, the same set as described above was used with compound concentrations from 0.02 to 150 μM . The log inhibitor vs. response (variable slope) algorithm of the GraphPad Prism software was used to fit the data.

5.3.4. Surface plasmon resonance (SPR)

To determine the binding constants of recombinant FUBP1 (HEK293T expression system) to *FUSE p21*, SPR buffer (50 mM Tris pH 7.4, 100 mM NaCl, 0.1% BSA, 0.01% Surfact Amp) was used, and all experiments were performed with a chip temperature of 25 °C. *FUSE* DNA was immobilized on a Proteon[™] NLC sensor chip (*BioRad Laboratories*, Munich, Germany) surface, which was coated with a layer of NeutrAvidin. Chips were activated by air initialization and the specific SPR preconditioning program for NLC chips. 2.5 nM and 5 nM *FUSE p21* DNA were diluted in SPR buffer and incubated with the chip surface at a flow rate of 30 $\mu\text{l}/\text{min}$ for 120 s. This resulted in approximately 30 and 60 RUs immobilized ligand, respectively. Additionally, a non-FUBP1 binding *FUSE* sequence, *FUSE p31*,¹ was used as a negative control, immobilized on the same chip but another channel. This channel was used as the background for unspecific interaction of FUBP1 with the chip surface and served as a normalization standard.

A dilution series of FUBP1 (0.2–50 nM) was used to determine optimal screening conditions. The dissociation constant (K_D) was calculated using the equilibration mode. For this analysis, the response units at the end of the association phase (equal with the amount of *FUSE p21*-bound FUBP1) were plotted against the FUBP1 concentration used and fitted.

After verification of the functionality of the expressed and purified FUBP1 protein, small molecules were included in the liquid phase of SPR experiments to investigate their effect on the binding between FUBP1 and *FUSE p21*. As SPR technology measures the binding of analyte and ligand based on surface size changes, colored small molecules do not interfere with this assay. In general, 5 nM *FUSE* (*p21* and *p31*) was used as a ligand and 25 nM FUBP1 as the analyte. All experiments were performed with a flow rate of 120 $\mu\text{l}/\text{sec}$, an association phase of 120 s and a dissociation phase of 300 s. In contrast to the binding constant determination for FUBP1/*FUSE p21*, 1% DMSO was included for the small molecule screening set up to minimize the effect of the compounds solvent.

Prior to the experiments, the chip was equilibrated with this buffer for half an hour, until no change in response units was observed. Furthermore, a corresponding DMSO control (including 25 nM FUBP1) to define the maximal binding of FUBP1 to *FUSE p21* was added. This lane was set at 100% for IC_{50} determination of compounds.

In a first screening approach, all tested small molecules (final concentration of 200 μM) were preincubated with 25 nM FUBP1. Potential inhibitors (positive hits) were subsequently tested with a concentration of 50 μM to exclude false positives. IC_{50} determination was performed in two subsequent experiments, with concentrations ranging from 0.01 to 100 μM . After background subtraction, response units at the end of the dissociation phase were normalized to the corresponding DMSO control and plotted against the logarithmic compound concentration. The resulting curves were fitted using the log inhibitor vs. response (variable slope) algorithm of the GraphPad Prism software. Binding graphs were recorded using the BioRad ProteOn[™] XPR 36 device (*BioRad Laboratories*).

5.3.5. qRT-PCR analysis of FUBP1 target genes

1×10^6 Hep3B cells were seeded prior to incubation with 5–50 μM pyrazolo[1,5a]pyrimidine derivatives. After 6 h, cells were harvested and RNA was extracted using the RNeasy[®] Mini Kit from *Qiagen GmbH* (Hilden, Germany). On-column DNA digestion was performed to exclude DNA contaminations. Subsequently, 1.5 μg RNA were transcribed into cDNA using the Omniscript[®] Reverse Transcription Kit (*Qiagen*). qRT-PCR was performed using SYBR[®] green master mix (*Thermo Scientific*). Analysis of mRNA expression levels was performed using the following qPCR-primer pairs:

hu <i>p21</i> for	5'-TGG AGA CTC TCA GGG TCG AAA-3'
hu <i>p21</i> rev	5'-CCG GCG TTT GGA GTG GTA-3'
hu <i>BIK</i> for	5'-CTT GAT GGA GAC CCT CCT GTA TG-3'
hu <i>BIK</i> rev	5'-AGG GTC CAG GTC CTC TTC AGA-3'
hu <i>CCND2</i> for	5'-CTC TGC TGA GCG GTA CTA AAC-3'
hu <i>CCND2</i> rev	5'-CTC CCT TCA ACT ATC ATC CCA TAC-3'
hu <i>GAPDH</i> for	5'-AAT GGA AAT CCC ATC ACC ATC T-3'
hu <i>GAPDH</i> rev	5'-CGC CCC ACT TGA TTT TGG-3'

5.3.6. Cell expansion assay

This assay was performed to evaluate the influence of compound treatment on the expansion potential of HCC cell lines. For each condition, 1×10^5 adherent cells were treated either with DMSO (solvent control), 10 or 20 μM compound **6** or remained untreated (untreated control). Medium and compound were exchanged daily to ensure sufficient nutrition supply and stability of the compound. Cells were counted at the time points 0 h, 24 h, 48 h and 72 h, respectively. For each time point, the cell count was determined in technical duplicates using a Neubauer improved hemocytometer (*Marienfeld Superior*, Darmstadt, Germany). Dead cells were excluded using trypan blue (0.4%; *GIBCO*, Eggenstein, Germany) staining. All experiments were performed in biological triplicates.

5.3.7. Nicoletti assay

For cell cycle and cell death analyses Nicoletti assays were performed as described previously.²⁷ Treated cells and the cell culture supernatant were collected in FACS tubes. Adherent cells were harvested using 0.05% trypsin-EDTA. Cells were pelleted at 4 °C and

200×g for 5 min. Immediately after aspiration of the supernatant, cells were fixed in 70% ice-cold ethanol under constant vortexing. Fixed cells were stored for at least 24 h and up to two weeks at 4 °C.

Prior to staining, ethanol was exchanged against 38 mM sodium citrate (pH 7.4). Afterwards, cells were incubated with 50 µl propidium iodide (PI) staining solution (38 mM sodium citrate pH 7.4, 50 µg/ml PI and 50 µg/ml RNase A) for 20 min in the dark. Fluorescence intensity in the FL2 channel at 585 nm was measured and depicted as FL2-A against FL2-W. Recorded FACS data were analyzed using the Sync Wizard tool of the ModFit LT software from *Verity Software House*.

For the determination of dead cell ratios, Hep3B, HepG2 and Huh7 cells were treated with DMSO control, Methanol control, 10 or 20 µM compound **6**, mitomycin c (MMC; *Roche*, Mannheim, Germany; dissolved in MeOH; 4 µg/ml for Hep3B cells, 1 µg/ml and 2 µg/ml for HepG2 cells and 1 µg/ml for Huh7 cells), 2.5 µM doxorubicin (DOX; *Sigma-Aldrich*; dissolved in DMSO) and combinations of compound **6**, MMC and DOX. 24 h after treatment, cells were harvested and fixed.

5.3.8. Software analysis

5.3.8.1. Statistical analyses and determination of synergism. The inhibitory concentrations of tested compounds were calculated using the log inhibitor vs. response (variable slope) fit of the GraphPad Prism software. Statistical significances of mRNA fold changes and expansion assays were calculated using the unpaired, two-tailed student's *t* test.

Synergism of compound combinations was assigned using the *response additivity* approach by Slinker,²⁵ assuming that synergistic effects of the double treatments exceed a theoretical additive effect of two single concentrations. A *combination index* (CI) <1 indicates synergism, =1 additivity and >1 antagonism of compound combinations. All depicted CIs were calculated from three independent experiments.

Statistical significance of single concentration combinations was assessed using the two-way analysis of variance (ordinary two-way ANOVA).²⁵ *p* values of <0.05 (*), *p* <0.01 (**), *p* <0.001 (***) and *p* <0.0001 (****) were considered statistically significant.

5.3.8.2. Activity cliff analysis of the SAR landscape. 2D structures of tested SAR compounds were aligned to the lead structure compound **1** using the Forge simulation software from Cresset (Cambridgeshire, United Kingdom). Activity cliffs were assigned using the *Activity Atlas* tool, and the in-software application *Activity Minor* served for the assignment of disparity values and comparative field analyses of the investigated compounds.

Funding

This work was supported by the German Cancer Consortium and the German Cancer Aid (M.Z.; No. 109327 and 70112344) as well as by the Else-Kröner-Fresenius Foundation graduate college for Translational Research Innovation–Pharma (TRIP). K.H. expresses thanks to the graduate college for Translational Research Innovation–Pharma (TRIP) for the Ph.D. fellowship.

Authors' contributions

SH: acquisition, analysis and interpretation of assay data, FORGE analysis of SAR study compounds; design and generation of display items, drafting of the manuscript KH: synthesis of candidate compounds and interpretation of data, generation of display

items, drafting of the manuscript. SKH: Establishment of binding assays and accomplishment of initial medium throughput screening; JA: evaluation of the initial screening compounds. RB, EP, MZ and DO: conceiving of the study; experimental design, critical reading and correction of the manuscript. All authors read and agreed to the final manuscript.

Acknowledgements

We want to acknowledge Susanne Bösser for excellent technical assistance and Markus Braner for support and maintenance of the SPR device. The initial screening was performed in the Research Group PhosphoSites, Goethe University of Frankfurt/Main.

A. Supplementary data

Supplementary data associated with this article can be found, in the online version, at <http://dx.doi.org/10.1016/j.bmc.2016.09.015>.

References and notes

- Rabenhorst, U.; Beinoraviciute-Kellner, R.; Brezniceanu, M. L.; Joos, S.; Devens, F.; Lichter, P.; Rieker, R. J.; Trojan, J.; Chung, H. J.; Levens, D. L.; Zornig, M. *Hepatology* **2009**, *50*, 1121.
- Malz, M.; Bovet, M.; Samarin, J.; Rabenhorst, U.; Sticht, C.; Bissinger, M.; Roessler, S.; Bermejo, J. L.; Renner, M.; Calvisi, D. F.; Singer, S.; Ganzinger, M.; Weber, A.; Gretz, N.; Zornig, M.; Schirmacher, P.; Breuhahn, K. *Hepatology* **2014**, *60*, 1241.
- Malz, M.; Weber, A.; Singer, S.; Rieher, V.; Bissinger, M.; Riener, M. O.; Longerich, T.; Soll, C.; Vogel, A.; Angel, P.; Schirmacher, P.; Breuhahn, K. *Hepatology* **2009**, *50*, 1130.
- Zubaidah, R. M.; Tan, G. S.; Tan, S. B.; Lim, S. G.; Lin, Q.; Chung, M. C. *Proteomics* **2008**, *8*, 5086.
- de Wit, M.; Kant, H.; Piersma, S. R.; Pham, T. V.; Mongera, S.; van Berkel, M. P.; Boven, E.; Ponten, F.; Meijer, G. A.; Jimenez, C. R.; Fijneman, R. J. *Proteomics* **2014**, *99*, 26.
- Humar, B.; Graziano, F.; Cascinu, S.; Catalano, V.; Ruzzo, A. M.; Magnani, M.; Toro, T.; Burchill, T.; Futschik, M. E.; Merriman, T.; Guilloford, P. *Oncogene* **2002**, *21*, 8192.
- Zhang, F.; Tian, Q.; Wang, Y. *Onkologie* **2013**, *36*, 650.
- Tang, Q.; Xia, W.; Ji, Q.; Ni, R.; Bai, J.; Li, L.; Qin, Y. *Int. J. Clin. Exp. Pathol.* **2014**, *7*, 2019.
- Lasserre, J. P.; Fack, F.; Revets, D.; Planchon, S.; Renaud, J.; Hoffmann, L.; Gutleb, A. C.; Müller, C. P.; Bohn, T. *J. Proteome Res.* **2009**, *8*, 5485.
- Xu, S. G.; Yan, P. J.; Shao, Z. M. *J. Cancer Res. Clin. Oncol.* **2010**, *136*, 1545.
- Ding, Z.; Liu, X.; Liu, Y.; Zhang, J.; Huang, X.; Yang, X.; Yao, L.; Cui, G.; Wang, D. *Mol. Carcinog.* **2015**, *54*, 405.
- Baumgarten, P.; Harter, P. N.; Tonjes, M.; Capper, D.; Blank, A. E.; Sahm, F.; von Deimling, A.; Kolluru, V.; Schwamb, B.; Rabenhorst, U.; Starzetz, T.; Kogel, D.; Rieker, R. J.; Plate, K. H.; Ohgaki, H.; Radlwimmer, B.; Zornig, M.; Mittelbronn, M. *Neuropathol. Appl. Neurobiol.* **2014**, *40*, 205.
- Hsiao, H. H.; Nath, A.; Lin, C. Y.; Folta-Stogniew, E. J.; Rhoades, E.; Braddock, D. T. *Biochemistry* **2010**, *49*, 4620.
- Zhang, J.; Chen, Q. M. *Oncogene* **2013**, *32*, 2907.
- Rabenhorst, U.; Thalheimer, F. B.; Gerlach, K.; Kijonka, M.; Bohm, S.; Krause, D. S.; Vauti, F.; Arnold, H. H.; Schroeder, T.; Schnutgen, F.; von Melchner, H.; Rieger, M. A.; Zornig, M. *Cell Rep.* **2015**, *11*, 1847.
- Jang, M.; Park, B. C.; Kang, S.; Chi, S. W.; Cho, S.; Chung, S. J.; Lee, S. C.; Bae, K. H.; Park, S. G. *Oncogene* **2009**, *28*, 1529.
- Vindigni, A.; Ochem, A.; Triolo, G.; Falaschi, A. *Nucleic Acids Res.* **2001**, *29*, 1061.
- Huth, J. R.; Yu, L.; Collins, I.; Mack, J.; Mendoza, R.; Isaac, B.; Braddock, D. T.; Muchmore, S. W.; Comess, K. M.; Fesik, S. W.; Clore, G. M.; Levens, D.; Hajduk, P. J. *J. Med. Chem.* **2004**, *47*, 4851.
- Emelina, E. E. P.; Petrov, A. A.; Selivanov, S. I.; Filyukov, D. V. *Russ. J. Org. Chem.* **2008**, *2*, 251.
- Ji, Y.; Trenkle, W. C.; Vowles, J. V. *Org. Lett.* **2006**, *8*, 1161.
- Puterová, Z.; Andicsová, A.; Vég, D. *Tetrahedron* **2008**, *64*, 11262.
- Kim, B. R.; Lee, H. G.; Kang, S. B.; Jung, K. J.; Sung, G. H.; Kim, J. J.; Lee, S. G.; Yoon, Y. J. *Tetrahedron* **2013**, *69*, 10331.
- Singh, S. P.; Kapoor, J. K.; Kumar, D.; Threadgill, M. D. *J. Fluorine Chem.* **1997**, *83*, 73.
- Emelina, E. E.; Petrov, A. A.; Firsov, A. V. *Russ. J. Org. Chem.* **2001**, *6*, 825.
- Slinker, B. K. *J. Mol. Cell. Cardiol.* **1998**, *30*, 723.
- Studier, F. W. *Protein Expr. Purif.* **2005**, *41*, 207.
- Riccardi, C.; Nicoletti, I. *Nat. Protoc.* **2006**, *1*, 1458.